Effect of selective post-aging treatment on subsurface damage of quasicrystal reinforced Al composite manufactured by selective laser melting

N. Kang[a,c,*], M. El Mansori[b,d], J.L. Lu[a,c], X. Lin[a,c], W.D. Huang[a,c]

[a] State Key Laboratory of Solidification Processing, Northwestern Polytechnical University, Xi'an, Shaanxi 710072, PR China
[b] MSMP Laboratory, EA-7350, Arts et Metiers ParisTech, Aixen Provence 13617, France
[c] Key Laboratory of Metal High Performance Additive Manufacturing and Innovative Design, MIIT China, Northwestern Polytechnical University, Xi'an, Shaanxi 710072, PR China
[d] Texas A&M Engineering Experiment Station, College Station, TX 77843, USA

Keywords:
Heat treatment
Selective laser melting
Metal matrix composite
Quasicrystal
Compression

A B S T R A C T

In this work, Al-Fe-Cr quasicrystal reinforced Al matrix composite was in-situ prepared by using selective laser melting from powder mixture of Al-Cu-Fe-Cr quasicrystal and pure Al. The effect of selective post-aging treatment on microstructure and mechanical properties were determined with focus on the metastable phases. The microstructural analysis, which was determined by X-ray diffraction and scanning electron microscopy, indicates that the Al-based intermetallic is precipitated from supersaturated α-Al after the aging process. Moreover, the compression tests were performed on the samples in form of dense and lattice structures (50% porosity). The elastic modules of dense and lattice structural samples reduce from 21.3 GPa and 4.4–14.6 GPa and 3.6 GPa by using a low cooling-rated aging process. After aging process, the compressive deformation behavior of dense part changes from elastic-plastic-fracture mode to elastic-plastic-densification mode. On the other hand, the failure mechanism of lattice structural sample changes from rapid-single-stage to slow-double-stage with an improvement of the strain at failure.

1. Introduction

Metal matrix composites (MMCs) have been extensively studied during the past few decades, because they combine the high strength and hardness of reinforcement and good damage tolerance of metal matrix. Thanks to the low density, high strength/weight ratio, high corrosion resistance and low cost, aluminum and its alloys are frequently considered as matrix material in MMCs [1]. In general, according to the work of Deuis et al. [2], the reinforcement in MMCs should possesses high hardness and stiffness for obtaining high mechanical strength and ductility, for instance, ceramic TiB_2 [3], WC [4], Al_2O_3 [5] and TiN [6] etc. But, in physical, there is a big difference in thermal and crystalline properties between ceramic and metal materials, which causes the interfacial problems with performance reduction of MMCs. Recently, the emerge of high strength and hardness metal-based reinforcement, such as metallic glass [7], quasicrystal [8] and high-entropy alloy [9], overcomes those drawbacks by solving the interfacial problem. Additionally, the metal-based reinforcements are also possible to be in-situ formed during the preparation of MMCs with strong metallurgical bonding [10].

Selective laser melting (SLM), as one of important additive manufacturing process, shows great potential application in producing the metallic component with extremely high complex form [11,12]. In this process, the metallic powder sized between several to one hundred micrometers is spread out with preferred layer thickness. Then, the powder bed is selectively fused by using high energy laser beam, which is controlled by a galvo system. With the descend of workbench for one layer thickness, the process mentioned above is repeated with new laser scanning strategy until the 3D component is successfully prepared [13]. Moreover, the layer by layer production procedure is irreplaceable in the elaboration of novel composite materials with homogenous microstructure, which cannot be easily prepared by conventional casting and process [14]. Until now, SLM process is used to produce various kind of MMCs based on Fe [15], Al [16], Ti [17] and Ni [18] matrix. On the other hand, the high cooling rate of SLM process leads to an ultra-fine microstructure feature, which causes different higher mechanical strength than conventional casted samples [19,20].

Our previous work investigated on the SLM process of quasicrystal

* Corresponding author at: State Key Laboratory of Solidification Processing, Northwestern Polytechnical University, Xi'an, Shaanxi 710072, PR China.
E-mail address: nan.kang@nwpu.edu.cn (N. Kang).

[21] and their composite [22,23] and reported that a dense, high wear resistance and strength quasicrystal reinforced α-Al composite was successfully in-situ prepared by using SLM process from powder mixture. As one kind of thermal sensible materials, post heat treatment and cooling condition, such as cooling method, are important and essential for quasicrystal reinforcement and supersaturated α-Al matrix. On the other hand, selective post-aging treatment is an adopted strategy for decreased or increased subsurface damage under mechanical loading, which is a result of the most pronounced manifestation of mechano-chemistry and physico-chemistry of the SLM process under boundary cooling conditions. However, to the best of authors' knowledge, no work has been done in this field. Thus, in this work, the effects of selective post-aging treatment on microstructure, compression properties and subsurface damage behavior of quasicrystal reinforced Al composite manufactured by using SLM were investigated.

2. Experimental details

2.1. Materials

The home-made (LERMPS-UTBM, France) spherical pure Al powder and $AlCu_{20}Fe_{10}Cr_5$ powder, which were mechanical mixed with weight proposition of 7:3 in a tumbling mixer for 120 min ((TURBULA, Switzerland)), were used in this work. The surface morphology of powder mixture is shown in Fig. 1(a). It is worth to note that the gas-atomized quasicrystal powder presents a rough surface consisted by small fragment (seen in Fig. 1(b)). More information about the feedstock materials can be found in our previous works [21,22]. The samples were deposited on a sand-blasted pure Al substrate with dimension of 250 × 250 × 20 mm^3.

2.2. SLM methodology

In this work, both the cubic dense and lattice structural samples (15 × 15 × 15 mm^3) were prepared by using a commercial available SLM system (SLM 250, SLM solution, Germany). This system is equipped with YLR-100-SM single-mode CW ytterbium fiber laser and f-θ scanning instrument. The maximum laser power and scanning speed reach to 400 W and 5000 mm/s. The process parameters for obtaining defect-free sample, which have been optimized by our previous work [23], are listed in Table 1. In order to avoid the oxidation behavior during laser melting process, all the pre-heating, proceeding and cooling processes are performed under high pure argon atmosphere with 1 bar pressure. The oxygen content was controlled inferior 0.2 vol % during SLM process. The as-fabricated dense and lattice samples are shown in Fig. 1(c and d). The lattice structure consists by *bcc* cellular with size of 2.5 × 2.5 × 2.5 mm^3. The heat treatment was performed on a vacuum heat treatment instrument (CTJZH, China) for 30 min at 450 °C, followed by water cooling (WC, quenching), air cooling (AC) or furnace cooling (FC, about 6 h) to ambient temperature.

2.3. Characterizations

The crystallization state of the samples was examined using X-ray diffraction (X' Pert MPD PRO, XRD), which was performed with a Cu Kα radiation operated at 40 kV and 35 mA. For the over and local views analysis, the X-ray scanning speeds are set as 10°/min and 1°/min, respectively. Metallographic samples were prepared by mechanical and OP-S polishing. A Keller solution was used as etching agent. Then the microstructures were characterized by optical microscopy (OM) (Keyence VH-Z50L) and scanning electron microscopy (SEM) (Tescan VEGAIILMH), equipped with an Ican energy-dispersive X-ray spectrometer (EDS). A compressive material testing instrument (INSTRON, USA) was employed to perform the compression test with a constant

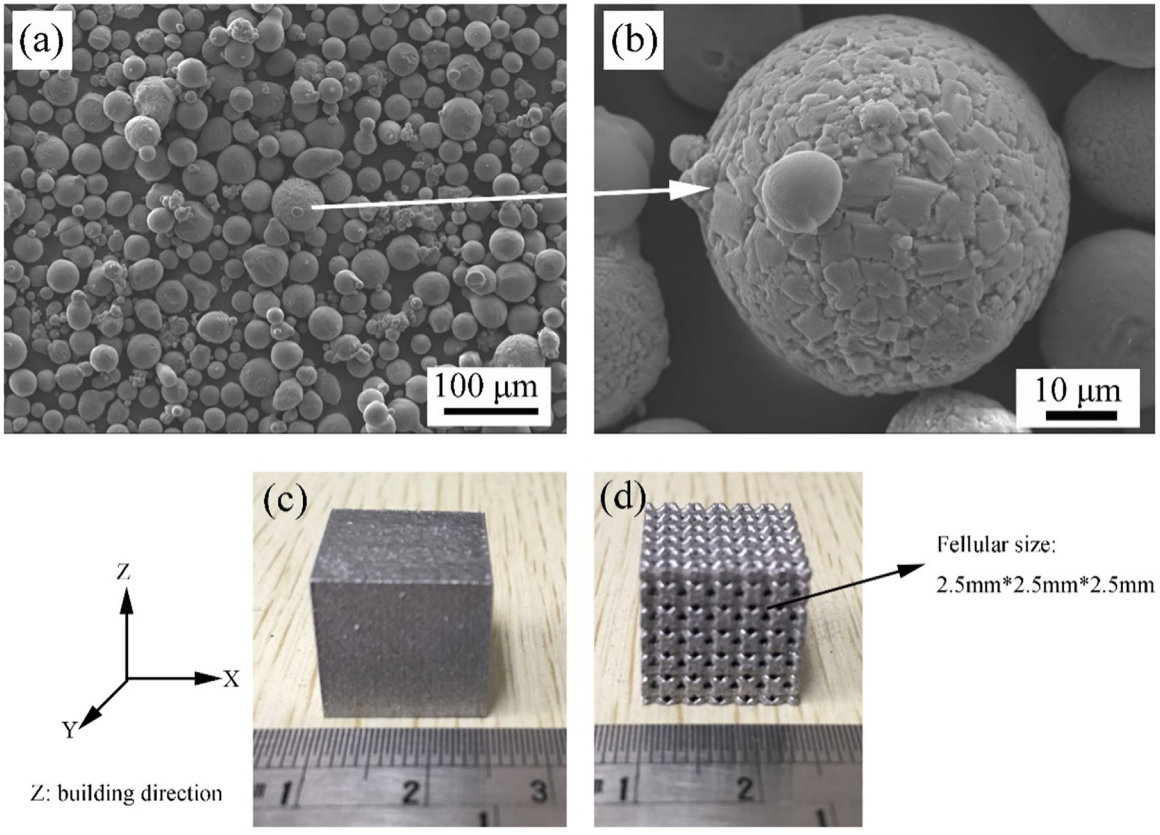

Fig. 1. (a) Surface morphology of powder mixture and (b) Quasicrystal powder, SLM processed (c) Dense and (b) Lattice structural samples.

Table 1
Optimized process parameters used in this work.

Parameter	Laser power	Laser scanning speed	Layer thickness	Hatch distance	Substrate temperature
Value	300 W	2000 mm/s	50 μm	120 μm	80 °C

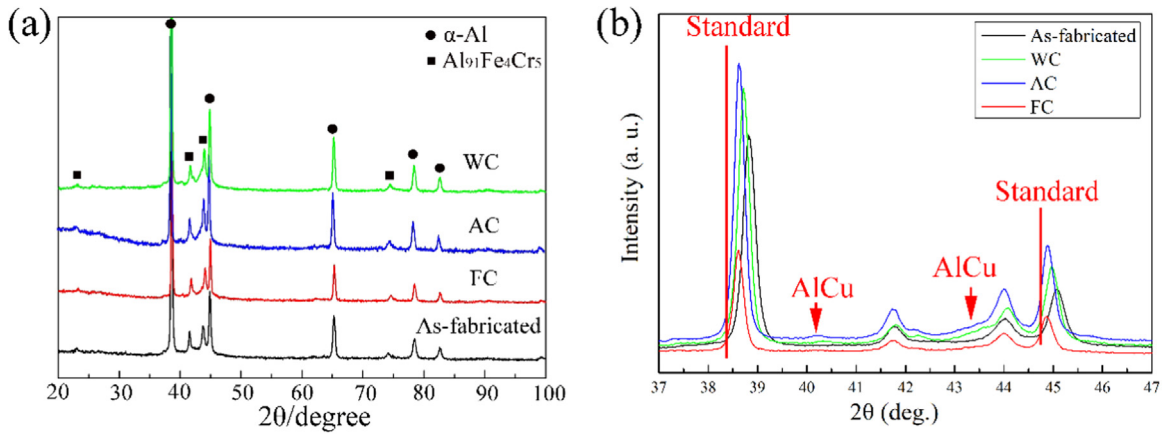

Fig. 2. (a) high scanning speed overview and (b) low scanning speed local-view XRD patterns of SLM processed composite under several cooling conditions.

traverse speed of 0.05 mm/min. The dense sample presents a cylindrical dimension: diameter of 6 mm and length of 9 mm (building direction). Additionally, compression test was directly performed on cubic lattice sample along building direction.

3. Results and discussion

Fig. 2 presents the XRD patterns of SLM processed composite sample at as-fabricated, water cooling, air cooling and furnace cooling conditions. From the overview pattern in Fig. 2(a), it can be seen that all the SLM processed composite samples with or without heat treatment present a mixture phase of α-Al and $Al_{91}Fe_4Cr_5$ quasicrystal [22]. Moreover, no marked modification in characteristic phase or peak intensity is noted between as-fabricated and heat-treated samples under different cooling conditions. The detailed analysis with the low X-ray scanning speed, as seen in Fig. 2(b), shows that a slight movement to left side of α-Al phase after heat treatment, such as Al (1 1 1) and Al (2 0 0) planes. The accurate positions of those two lattice planes are summarized in Table 2.

According to reference [24], the cooling rate, mentioned in this study, presents an order as follow: as-fabricated > water cooling > air cooling > furnace cooling. Our previous results of transmission electron microscopy (TEM) illustrate a substitutional supersaturated α-Al (Cu) in SLM processed composite sample [23]. This substitutional supersaturated behavior leads to the lattice distortion by reducing the lattice constant, due to the small atomic size of copper element [25]. Therefore, after heat treatment process with low cooling rate, the copper precipitates from Al-matrix with a decrement of the degree of supersaturation. It causes an improvement of lattice constant and diffraction peak movement to the left side (see in Fig. 2(b) and Table 2). It is worth to note that all the α-Al peaks of the SLM processed sample locate at right side of diffraction peak of standard pure Al, given to the solid solution of Cu element in Al matrix. Additionally, after selective post-aging treatment, the copper, which precipitates from Al matrix, form Al-Cu intermetallic (seen in Fig. 2(b)).

Table 2
Accurate positions of Al (1 1 1) and Al (2 0 0) lattice planes in standard card and SLM processed composite at as-fabricated and heat treated condition.

Lattice plane	Standard card	As-fabricated	Water cooling	Air cooling	Furnace cooling
(1 1 1)	38.472	38.820	38.720	38.619	38.619
(2 0 0)	44.738	45.103	44.970	44.869	44.869

The microstructures at low and high magnifications of SLM processed composite sample at as-fabricated, water cooling, air cooling and furnace cooling conditions are shown Fig. 3 and Fig. 4. As seen in Fig. 3, the as-fabricated and heat treated samples shows a special conchoidal microstructure consisted by Al-rich region (light region in Figure) and quasicrystal reinforced Al matrix composite (dark region in Figure). The formation of this conchoidal structure is contributed to the use of powder mixture as feedstock materials. During SLM process, the laser beam can be focused into very small size, which tends to produce a small molten pool with ultra-high cooling rate. Thus, the non-uniformed elemental distribution in meso-scale, in a way of conchoidal structure, appears inner and between laser traces (see in Fig. 3(a)). The area fraction of Al-rich region of the SLM processed sample with or without heat treatments, which is calculated by image analysis (Image J, USA) from 5 picture for 3 measurements, are shown in Fig. 3(e). After selective post-aging treatment process with water cooling, as shown in Fig. 3(b), the conchoidal structure can also be observed with slight reduction of Al-rich region from about 30–25%. Furthermore, in case of air cooled and furnace cooled samples, which possesses low cooling rate, the conchoidal structure reduces in certain extent to 12% and 7% respectively (Fig. 3(c, d and e)).

The OM and SEM images at high magnification are presented in Fig. 4 with emphasis on as-fabricated (high cooling rate) and furnace cooling (low cooling rate) conditions. Except the reduction of Al-rich region area, as shown in Fig. 4(a and b), it can be also observed that the morphology of dark reinforcement changes. SEM images in Fig. 4(c and d) show more information about the appearance of flocculent phase in case of low cooled samples. Combined with the results of XRD patterns, it can be reasonable concluded that the flocculent phase is Al-Cu intermetallic, which is precipitated from Al-matrix during the slow rate cooling procedure.

The Schematic illustration of microstructure evaluation during aging with high and low cooling rate is presented in Fig. 5. As shown in Fig. 5(a), the SLM processed composite presents a special conchoid structure at as-fabricated condition, which corresponds to Fig. 3(a). At the beginning of heat treatment, the sample was heat treated to 450 °C for 30 min. According the differential scanning calorimetry (DSC) analysis in our previous work [23] and Shih et. al [26], this

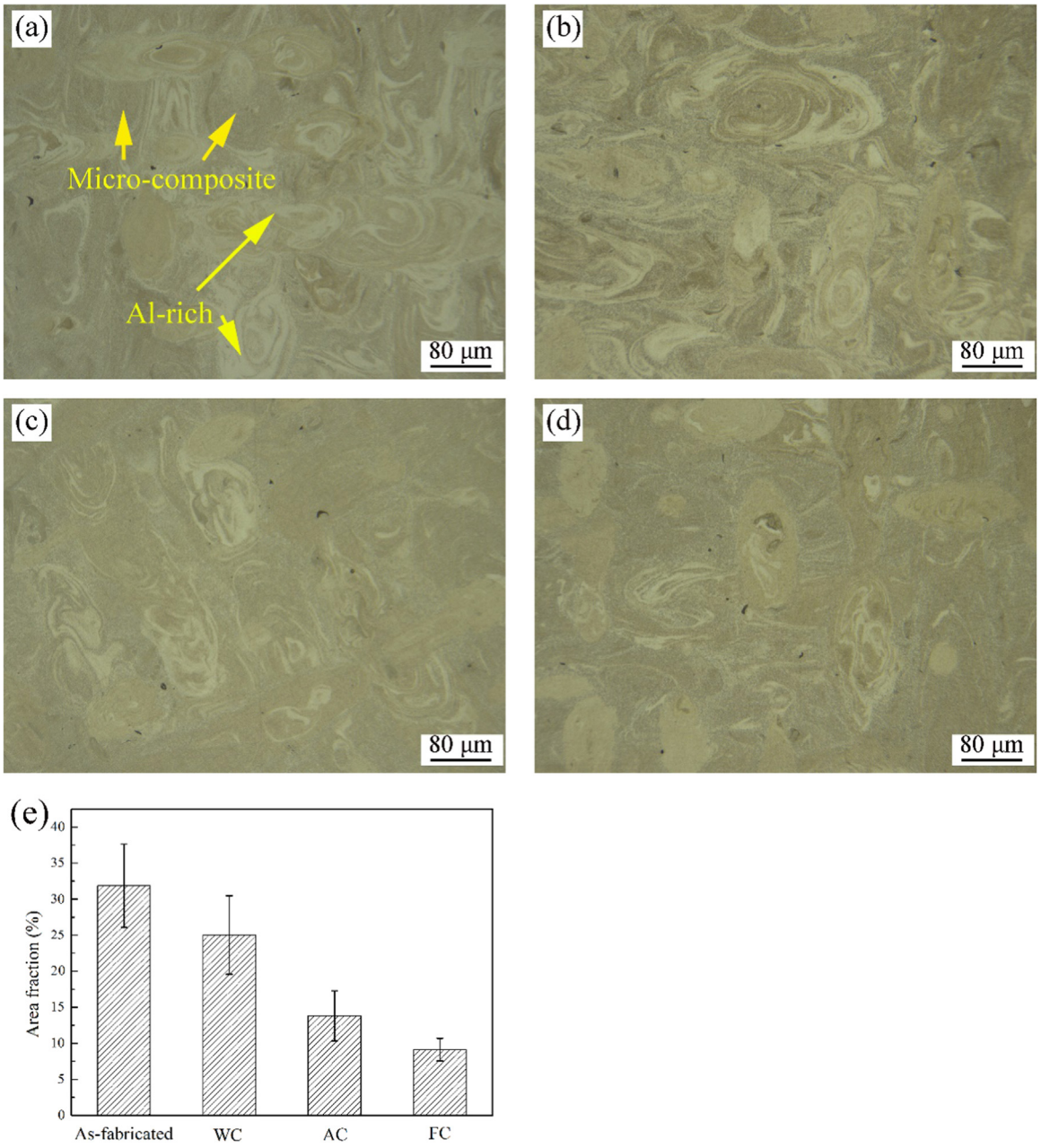

Fig. 3. OM images of microstructure of (a) as-fabricated, (b) water cooling (quenching), (c) air cooling and (d) furnace cooling composite samples, (e) area surface of Al-rich region.

temperature leads to appearance of Al-Cu rich region in supersaturated Al-rich region (seen in Fig. 5(b)). Depend on the cooling rate, the different transition behavior tends to form two microstructural features (seen in Fig. 5(c and d)). In case of high cooling rate (water cooling), some Cu element in Al-Cu rich region is quickly frozen into Al matrix after quenching process. Therefore, it presents a conchoidal structure with small amount of Al-Cu intermetallic in Al-rich region. On the other side, the Cu element will continuously precipitate from Al-matrix and enriches to form Al-Cu intermetallic phase. So, the Al-rich area in conchoidal structure is further reduced.

The compressive stress-strain curves of SLM processed composite samples under different cooling conditions in form of dense structure are shown in Fig. 6. The corresponding mechanical properties are summarized in Table 3. As shown in Fig. 6(a), the compressive behavior of SLM processed dense sample is significantly affected by heat treatment process. In details, as-fabricated dense sample presents a three-stage compressive mechanism: (I) elastic deformation; (II) plastic deformation and (III) crack-fracture. The crack-fracture appears at strain of 44.32% (see in Table 3). All three heat treated samples present a different behavior with emphasis on stage III, which changes from crack-fracture to densification. According to the work of Rosenthal et al. [27] in case of AlSi10Mg alloys, it indicates that the ductility of SLM processed dense sample is improved by using heat treatment by changing the fracture behavior. Meanwhile, modulus elastic, elastic limits and compression strength decreases from 21 GPa, 478 MPa and 1135 MPa to about 15 GPa, 400 MPa and 900 MPa respectively. Additionally, the “plastic modulus” (stage II) also significantly reduces after the heat treatment process. And this reduction in strength presents a negative relation with cooling rate of heat treatment.

The cross-sectional cracks inside of compressed as-fabricated composite (side view) are shown in Fig. 6(b). First of all, the macro-crack presents an intersection angle of 45° with building (loading) direction,

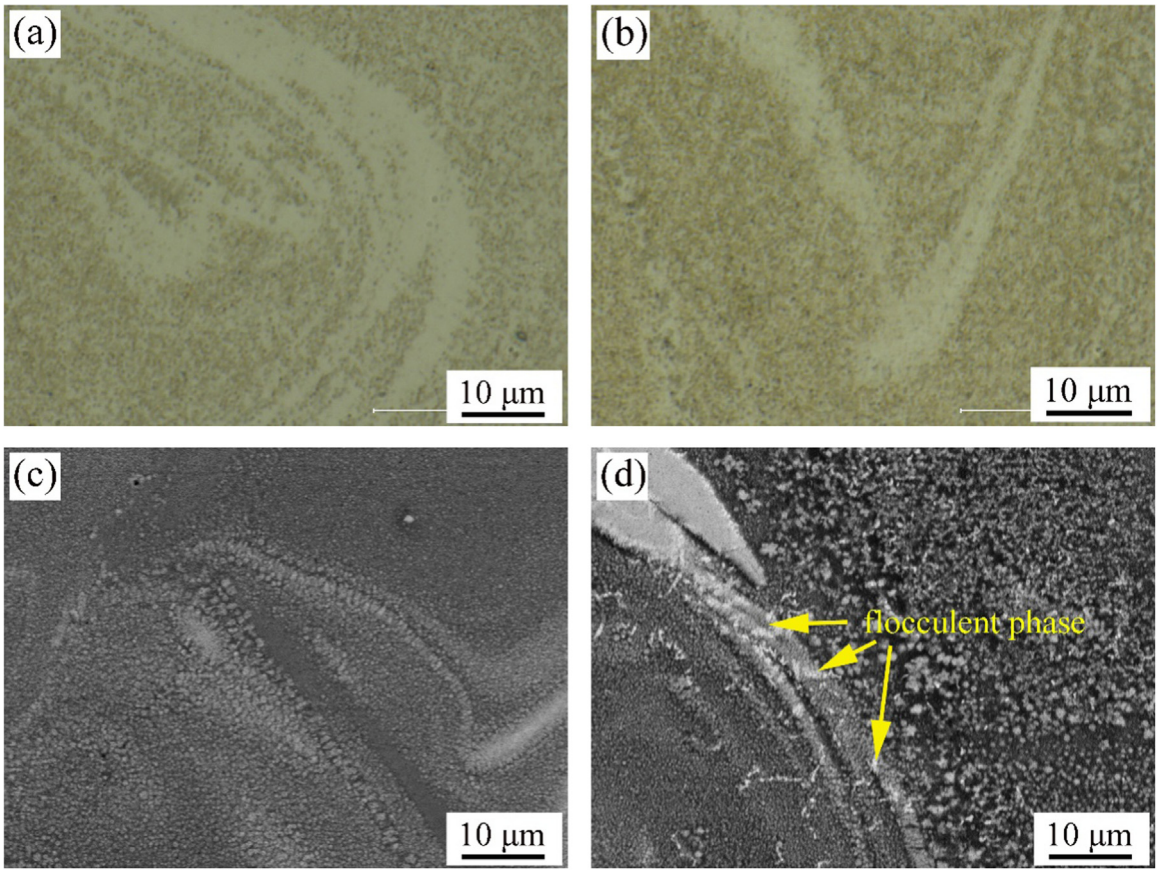

Fig. 4. Microstructure at high magnification of (a) as-fabricated (OM), (b) furnace cooling (OM), (c) as-fabricated (SEM) and (d) furnace cooling (SEM).

because it possesses maximum stress. Similar result was also reported by Pauly et al. in case of SLM processed metallic glass [28]. Additionally, the macro-crack tends to propagate through the Al-rich region, which can be attributed to two reasons. On the one hand, due to the lattice distortion of solid solution, the supersaturated α-Al shows high energy storage and low ductility [29]. On the other hand, in composite region, the quasicrystal phase presents high hardness, toughness and Young's Modulus [22,30], which can hold back the propagation of cracks. According to the work about fracture mechanics of Griffith [31], the critical stress for stable crack growth is:

$$\sigma_f = \sqrt{\frac{2E\gamma}{\pi\alpha}}$$

where, E is the Young's Modulus, γ is the surface energy per unit area and α is half of crack length. Therefore, the dark region (micro-composite), which possesses high Young's modulus and surface energy per

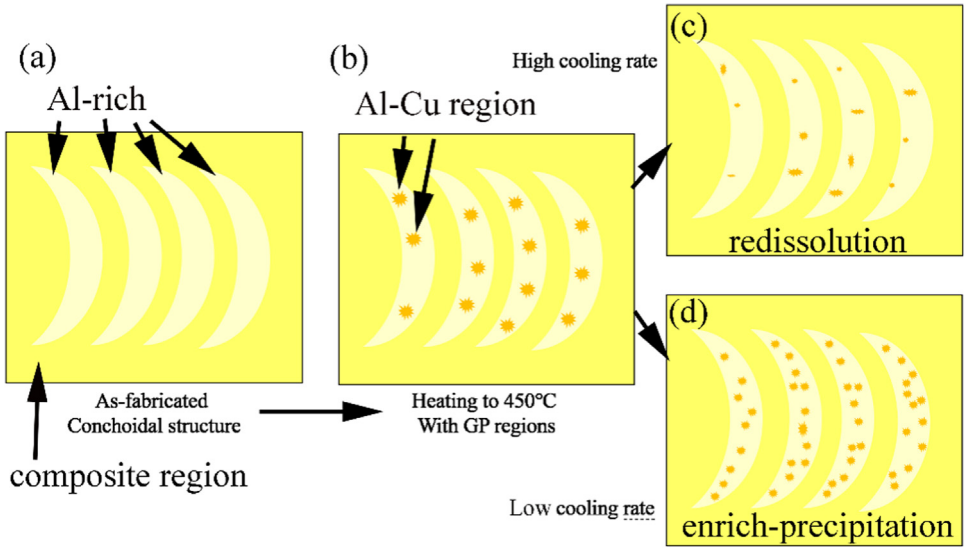

Fig. 5. Schematic illustration of microstructure evaluation during selective post-aging treatment under several cooling rate (water cooling: high cooling rate, air and furnace cooling: low cooling rate).

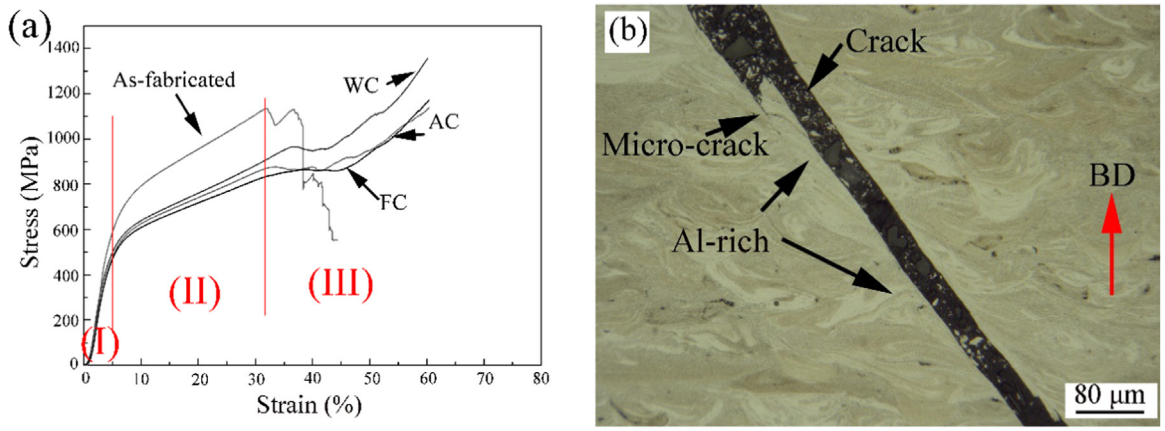

Fig. 6. (a) Compressive stress-strain curves of dense sample and (b) crack in as-fabricated sample (BD: building direction). (For interpretation of the references to color in this figure legend, the reader is referred to the web version of this article).

Table 3
compressive properties of SLM processed composite with several cooling conditions for dense structure.

Sample	Modulus(MPa)	Elastic limits (MPa)	Compression strength (MPa)	Crack-strain (%)
As-fabricated	21,253.70	478.06	1135.08	44.32
WC	14,441.66	419.81	964.23	–
AC	14,644.33	379.76	879.31	–
FC	14,981.49	369.59	864.68	–

unit area, shows high fracture stress of a material with a pre-existing crack of half-length α. In summary, it can be seen from Fig. 6(b) that some microcracks stop the propagation at dark regions (micro-composite). Thus, the macro-crack passes through the Al-rich region. After the heat treatment process, the degree of supersaturation reduces, which leads to an improvement in ductility of Al-rich region and homogeneity of microstructure. In addition, the precipitation of copper from Al-rich region leads to an increases of surface energy per unit. So, the macro-crack in heat treated samples can be avoided until 60% strain.

As mentioned in introduction part, Al-based material possesses low density and high toughness, which promotes the application of energy absorbing. On the other hand, the metal lattice structure, which can be easily produced by additive manufacturing technology, exhibits not only light in weight but also some unique functional characterizations, such as, low coefficient of heat transfer, high sound absorbing capacity, good crashworthiness and compression performance [32]. Therefore, the compression behavior of SLM processed composite samples with lattice structure is also determined and shown in Fig. 7. The as-fabricated and heat treated samples failure along 45° to load (building) direction after the compression test [33]. With the heat treatment, the composite sample presents an improvement in ductility and slight reduction of compression strength. The detailed values, as shown in Table 4, indicate the crack-strain increases from 4.91% to about of 6.25% after heat treatment under several cooling rates. In the point view of modulus, it decreases from 4.4 to 3.8 GPa following water cooling. With further decreasing the cooling rate, the modulus decreases to 3.6 GPa at air cooling and furnace cooling conditions.

The fractural morphology of SLM processed composite at as-fabricated and aging with furnace cooling conditions are shown in Fig. 8. In general, from the point view of microstructure, it can be seen the dimples appear on both the fractural surfaces, which indicates a plastic deformation induced ductile fracture. However, from the point view of mesostructure, the gap-like regions appeared on the fractural morphology of as-fabricated sample, differ from the stair-stepping fractural surface (as indicated by white arrows in Fig. 8(b)) of aged sample. Incorporated with stress-strain curves, the reason behind this is

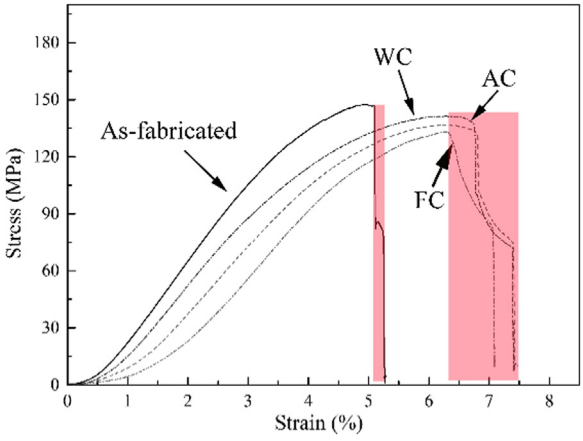

Fig. 7. Compressive stress-strain curves of lattice structural samples under several cooling conditions.

Table 4
compressive properties of SLM processed composite with several cooling conditions for lattice structure.

Sample	Modulus (MPa)	Elastic limits (MPa)	Compression strength (MPa)	Crack-strain (%)
As-fabricated	4379.84	120.95	147.47	4.91
WC	3845.25	102.09	141.38	6.29
AC	3633.06	109.10	136.74	6.28
FC	3661.30	111.22	133.19	6.25

attributed to different failure mechanisms in these two cases. As shown in Fig. 6 (red rectangle), the failure behavior of as-fabricated sample finishes in about 0.2% strain, which is much smaller than that of heat treated samples about of 1.0% strain. So, the crack in as-fabricated sample propagates rapidly across the Al-rich region. Due to the conchoidal structure feature of as-fabricated sample, the fractural surface presents a gap-like structure property. In contrast, the heat treated sample presents high ductility without failure during compression of dense sample (seen in Fig. 6) with homogenous microstructure. Therefore, it presents a typical stair-stepping fracture surface along the maximum stress direction (45° to loading direction), which is similar to the work of Zou et al. [32]. Moreover, the strain-stress curves of heat treated sample in Fig. 7 shows a two-steps failure mechanism: (I) slope-crack appearance and propagation and (II) cliff-stress concentration and failure.

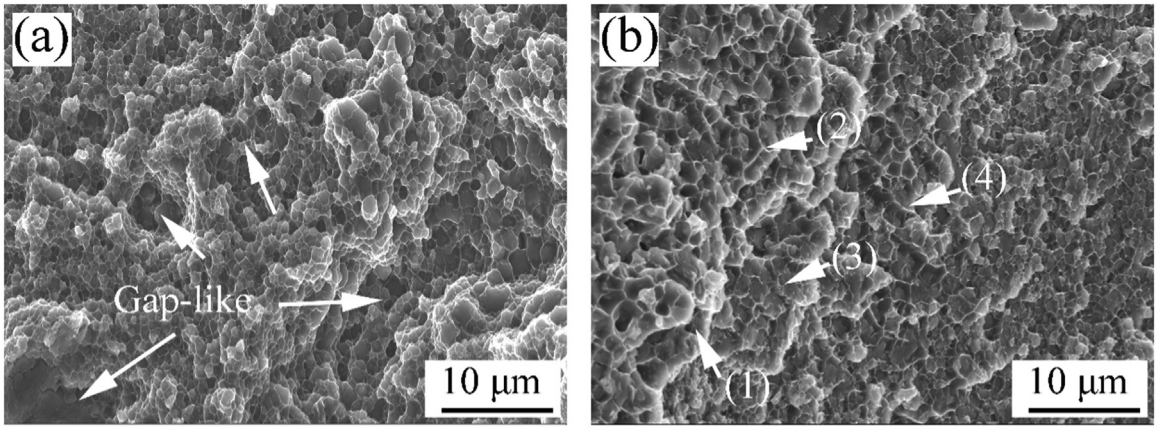

Fig. 8. Fracture surface morphology of SLM processed composite at (a) as-fabricated and (b) furnace cooled conditions (stage 1, 2, 3, 4 for altitude).

4. Conclusion

In this work, the effects of selective post-aging treatment on microstructure, compression properties and subsurface damage behavior of SLM processed quasicrystal reinforced Al composite were investigated on with focus on the powder mixture induced conchoidal structure and metastable phase. Several conclusions can be listed as follows:

(1) The Cu element precipitates from supersaturated Al(Cu) matrix during heating and perseveration processes, which was to form the Al-Cu intermetallic in following process at low cooling rate. Thus, the conchoidal structure in as-fabricated sample can be eliminated by using selective post-aging treatment with low cooling rate.
(2) The compression test results for dense sample indicates that the crack is inclined to pass though the Al-rich region in as-fabricated sample. Additionally, the selective post-aging treatment could reduce the cracking tendency in SLM processed composite by forming an homogenous microstructure. In details, it can be attributed to precipitation of Cu from supersaturated Al(Cu), which leads to reduction of lattice distortion. Thus, the ductility of composite system was improved.
(3) During the compression test, all lattice structural samples failure along the direction of maximum stress, 45° to building direction. With slight decreases in compressive strength, the ductility of lattice sample can be improved by selective post-aging treatment. Interestingly, the failure mechanism changes of one-step failure to two-step failure, given to selective post-aging treatment induced homogenization of microstructure and increment of crack propagation critical stress.

Acknowledgements

The work was supported by the National Key R&D Program of China (Grant No. 2016YFB1100100), National Natural Science Foundation (Grant No. 51604227) and Shaanxi Science & Technology Co-ordination & Innovation Project (Grant No. 2016KTZDCY02-02).

References

[1] I.A. Ibrahim, F.A. Mohamed, E.J. Lavernia, Particulate reinforced metal matrix composites — a review, J. Mater. Sci. 26 (1991) 1137–1156.
[2] R.L. Deuis, C. Subramanian, J.M. Yellup, Dry sliding wear of aluminium composite-a review, Compos. Sci. Technol. 57 (1997) 415–435.
[3] B. AlMangour, D. Grzesiak, J.-M. Yang, Rapid fabrication of bulk-form TiB2/316L stainless steel nanocomposites with novel reinforcement architecture and improved performance by selective laser melting, J. Alloy. Compd. 680 (2016) 480–493.
[4] N. Kang, W. Ma, L. Heraud, M. El Mansori, F. Li, M. Liu, H. Liao, Selective laser melting of tungsten carbide reinforced maraging steel composite, Addit. Manuf. 22 (2018) 104–110.
[5] Q. Han, Y. Geng, R. Setchi, F. Lacan, D. Gu, S.L. Evans, Macro and nanoscale wear behaviour of Al-Al 2 O 3 nanocomposites fabricated by selective laser melting, Compos. Part B Eng. 127 (2017) 26–35.
[6] H. Proudhon, J. Savkova, S. Basseville, V. Guipont, M. Jeandin, G. Cailletaud, Experimental and numerical wear studies of porous reactive plasma sprayed Ti–6Al–4V/TiN composite coating, Wear 311 (2014) 159–166.
[7] N. Kang, P. Coddet, H. Liao, C. Coddet, The effect of heat treatment on microstructure and tensile properties of cold spray Zr base metal glass/Cu composite, Surf. Coat. Technol. 280 (2015) 64–71.
[8] X. Guo, J. Chen, H. Yu, H. Liao, C. Coddet, A study on the microstructure and tribological behavior of cold-sprayed metal matrix composites reinforced by particulate quasicrystal, Surf. Coat. Technol. 268 (2015) 94–98.
[9] C. Huang, Y. Zhang, R. Vilar, J. Shen, Dry sliding wear behavior of laser clad TiVCrAlSi high entropy alloy coatings on Ti–6Al–4V substrate, Mater. Des. 41 (2012) 338–343.
[10] C.S. Ramesh, A. Ahamed, Friction and wear behaviour of cast Al 6063 based in situ metal matrix composites, Wear 271 (2011) 1928–1939.
[11] E.O. Olakanmi, R.F. Cochrane, K.W. Dalgarno, A review on selective laser sintering/melting (SLS/SLM) of aluminium alloy powders: processing, microstructure, and properties, Prog. Mater. Sci. 74 (2015) 401–477.
[12] D. Gu, C. Ma, M. Xia, D. Dai, Q. Shi, A. Multiscale, Understanding of the thermodynamic and kinetic mechanisms of laser additive, Manuf. Eng. 3 (2017) 675–684.
[13] L.E. Murr, S.M. Gaytan, D.A. Ramirez, E. Martinez, J. Hernandez, K.N. Amato, P.W. Shindo, F.R. Medina, R.B. Wicker, Metal fabrication by additive manufacturing using laser and electron beam melting technologies, J. Mater. Sci. Technol. 28 (2012) 1–14.
[14] N. Kang, W. Ma, F. Li, H. Liao, M. Liu, C. Coddet, Microstructure and wear properties of selective laser melted WC reinforced 18Ni-300 steel matrix composite, Vacuum 154 (2018) 69–74.
[15] M. Rombouts, J.P. Kruth, L. Froyen, P. Mercelis, Fundamentals of selective laser melting of alloyed steel powders, CIRP Ann. 55 (2006) 187–192.
[16] L. Thijs, K. Kempen, J.-P. Kruth, J. Van Humbeeck, Fine-structured aluminium products with controllable texture by selective laser melting of pre-alloyed AlSi10Mg powder, Acta Mater. 61 (2013) 1809–1819.
[17] B. Song, S. Dong, B. Zhang, H. Liao, C. Coddet, Effects of processing parameters on microstructure and mechanical property of selective laser melted Ti6Al4V, Mater. Des. 35 (2012) 120–125.
[18] T. Rong, D. Gu, Q. Shi, S. Cao, M. Xia, Effects of tailored gradient interface on wear properties of WC/Inconel 718 composites using selective laser melting, Surf. Coat. Technol. 307 (2016) 418–427.
[19] J. Zou, Y. Zhu, M. Pan, T. Xie, X. Chen, H. Yang, A study on cavitation erosion behavior of AlSi10Mg fabricated by selective laser melting (SLM), Wear 376–377 (2017) 496–506.
[20] N. Kang, P. Coddet, C. Chen, Y. Wang, H. Liao, C. Coddet, Microstructure and wear behavior of in-situ hypereutectic Al–high Si alloys produced by selective laser melting, Mater. Des. 99 (2016) 120–126.
[21] Y. Fu, N. Kang, H. Liao, Y. Gao, C. Coddet, An investigation on selective laser melting of Al-Cu-Fe-Cr quasicrystal: from single layer to multilayers, Intermetallics 86 (2017) 51–58.
[22] N. Kang, Y. Fu, P. Coddet, B. Guelorget, H. Liao, C. Coddet, On the microstructure, hardness and wear behavior of Al-Fe-Cr quasicrystal reinforced Al matrix composite prepared by selective laser melting, Mater. Des. 132 (2017) 105–111.
[23] N. Kang, M. El Mansori, X. Lin, F. Guittonneau, H. Liao, W.D. Huang, C. Coddet, In-situ synthesis of aluminum/nano-quasicrystalline Al-Fe-Cr composite by using selective laser melting, Compos. Part B 155 (2018) 382–390.
[24] U. Scipioni Bertoli, G. Guss, S. Wu, M.J. Matthews, J.M. Schoenung, In-situ characterization of laser-powder interaction and cooling rates through high-speed imaging of powder bed fusion additive manufacturing, Mater. Des. 135 (2017) 385–396.
[25] L. Pauling, The Nature of the Chemical Bond, 2nd ed., Cornell University Press, London, 1945.
[26] H.C. Shih, N.J. Ho, J.C. huang, Precipitation behaviors in Al-Cu-Mg and 2024

aluminum alloys, Metall. Mater. Trans. A 27A (1996) 2479–2494.
[27] I. Rosenthal, R. Shneck, A. Stern, Heat treatment effect on the mechanical properties and fracture mechanism in AlSi10Mg fabricated by additive manufacturing selective laser melting process, Mater. Sci. Eng. A 729 (2018) 310–322.
[28] S. Pauly, C. Schricker, S. Scudino, L. Deng, U. Kühn, Processing a glass-forming Zr-based alloy by selective laser melting, Mater. Des. 135 (2017) 133–141.
[29] X.P. Li, X.J. Wang, M. Saunders, A. Suvorova, L.C. Zhang, Y.J. Liu, M.H. Fang, Z.H. Huang, T.B. Sercombe, A selective laser melting and solution heat treatment refined Al–12Si alloy with a controllable ultrafine eutectic microstructure and 25% tensile ductility, Acta Mater. 95 (2015) 74–82.
[30] B.A. Sun, W.H. Wang, The fracture of bulk metallic glasses, Prog. Mater. Sci. 74 (2015) 211–307.
[31] A.A. Griffith, The phenomena of rupture and flow in solids, Philos. Trans. R. Soc. 221 (1921) 163–198.
[32] Y. Amani, S. Dancette, P. Delroisse, A. Simar, E. Maire, Compression behavior of lattice structures produced by selective laser melting: x-ray tomography based experimental and finite element approaches, Acta Mater. (2018).
[33] C. Li, H. Lei, Y. Liu, X. Zhang, J. Xiong, H. Zhou, D. Fang, Crushing behavior of multi-layer metal lattice panel fabricated by selective laser melting, Int. J. Mech. Sci. 145 (2018) 389–399.